# Mechanism of enhancement of ferroelectricity of croconic acid with temperature

**Sanghamitra Mukhopadhyay,*[a,f] Matthias J. Gutmann,[a] Mónica Jiménez-Ruiz,[b] Dominik B. Jochym,[c] Kjartan T. Wikfeldt,[d] Keith Refson,[a,e] and Felix Fernandez-Alonso [a,g]**

*Received Xth XXXXXXXXXX 20XX, Accepted Xth XXXXXXXXX 20XX*
*First published on the web Xth XXXXXXXXXX 200X*
**DOI: 10.1039/b000000x**

**A detailed study of the thermal behaviour of atomic motions in the organic ferroelectric croconic acid is presented in the temperature range 5 K-300 K. Using high-resolution inelastic neutron scattering and first-principles electronic-structure calculations within the framework of density functional theory and a quasiharmonic phonon description of the material, we find that the frequencies of the well defined doublet in inelastic neutron scattering spectra associated with out-of-plane motions of hydrogen-bonded protons decrease monotonically with temperature indicating weakening of these bonding motifs and enhancement of proton motions. Theoretical mean-square displacements for these proton motions are within 5% of experimental values. A detailed analysis of this observable shows that it is unlikely that there is a facile proton transfer along the direction of ferroelectric polarization in the absence of an applied electric field. Calculations predict constrained thermal motion of proton along crystallographic lattice direction $c$ retaining the hydrogen bond motif of the crystal at high temperature. Using the Berry-phase method, we have also calculated the spontaneous polarization of temperature dependent cell structures, and find that our computational model provides a satisfactory description of the anomalous and so far unexplained rise in bulk electric polarization with temperature. Correlating the thermal motion induced lattice strain with temperature dependent spontaneous polarizations, we conclude that increasing thermal strain with temperatures combined with constrained thermal motion along the hydrogen bond motif are responsible of this increase in ferroelectricity at high temperature.**

## 1 Introduction

Ferroelectricity in organic solids is a subject of increasing interest given its potential for applications across a number of situations of technological relevance.[1–10] In particular, the observation of above-room-temperature ferroelectricity [1,9] in the single-component molecular crystal croconic acid (hereafter CA), molecular formula $C_5O_5H_2$, has prompted a significant rethink of how carbon-based materials can develop and sustain a macroscopic electric polarization in the solid state.

The crystal structure of solid CA including the average position of all hydrogen (H) atoms has been determined previously using neutron diffraction (ND).[5–7] Figure 1 shows the crystal structure along two crystallographic directions, where it is to be noted that pentagonal units associated with distinct CA monomers are arranged into planar sheets having a width of about two molecular units on the $a-b$ plane. These hydrogen-bonded (HB) sheets extend indefinitely along the crystallographic $c$-axis, whereas the $a-b$ plane exhibits a characteristic accordion-like pattern. Topologically speaking, we can therefore distinguish between two types of HB environments depending on whether the corresponding H atoms reside on the hinges of the pleats or on the terraces between hinges, hereafter denoted as H(H) and H(T), respectively. From a molecular viewpoint, two OH groups are located on two adjacent carbon atoms on the same side of a given pentagonal carbon ring, and the two carbonyl oxygens on the opposite side are hydrogen-bonded to two different neighbouring CA molecules. The carbonyl oxygen at the apex of the pentagon between oxygen pairs

0[a] *ISIS Facility, Rutherford Appleton Laboratory, Chilton, Didcot, Oxfordshire, OX11 0QX, United Kingdom. E-mail: sanghamitra.mukhopadhyay@stfc.ac.uk*
0[b] *Institut Laue Langevin, 6 rue Jules Horowitz 38042, Grenoble Cedex 9, France*
0[c] *Scientific Computing Department, Rutherford Appleton Laboratory, Chilton, Didcot, Oxfordshire OX11 0QX, United Kingdom*
0[d] *University of Iceland, VR-III, Dunhaga 3, 107 Reykjavik, Iceland*
0[e] *Department of Physics, Royal Holloway, University of London, Egham TW20 0EX, United Kingdom*
0[f] *Imperial College London, Exhibition Road, London SW7 2AZ, United Kingdom.*
0[g] *Department of Physics and Astronomy, University College London, Gower Street, London WC1E 6BT, United Kingdom.*

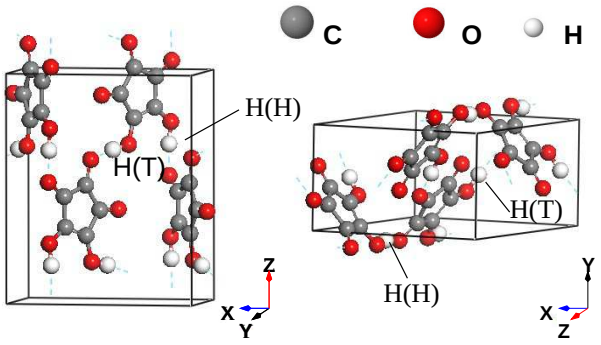


**Fig. 1** Unit cell of CA along the *b* (left) and *c* (right) crystallographic axes. For further details, see the text.

of HB donors and acceptors is too far away from neighbouring protons to participate in HB.

Crystalline CA has also been studied using $^{13}$C and $^{17}$O nuclear magnetic resonance (NMR).[11] An OH distance of 0.99±0.01 Å obtained from this work is consistent with ND results, evincing a very subtle difference in bond lengths (below 1%) for the two crystallographically distinct OH bonds present in CA.[5,6] This difference in OH distances are also consistent with results obtained from accurate X-ray charge density analysis.[12] Spectroscopic signatures of HBs have also been investigated using X-ray photoelectron spectroscopy (XPS)[13] and a combination of high-resolution inelastic neutron scattering (INS) experiments at liquid-helium temperatures and density functional theory (DFT) calculations.[5–7] In the latter case, HBs associated with H(H) and H(T) give rise to distinct and well-resolved spectral features around 900 cm$^{-1}$. These features are associated with proton motions transverse to the HB. From calculated Born-effective-charge tensors, the net electric polarization within the unit cell appears to be dominated by the presence of collinear HBs along the hinges. More specifically, these HB protons display anomalously high Born effective charges of around $3|e|$,[6,14] responsible for a strong 'push-pull' effect caused by electron-releasing and withdrawing groups along these HBs.[3] Formation of local domain has been predicted recently by analysing the observations of photoinduced polarisation switching.[8]

From a computational viewpoint, first-principles simulations of solid CA have also been reported using various DFT approaches,[1,3–9,14] including the use of state-of-the-art dispersion-corrected van-der-Waals functionals.[5,6,14,15] From these calculations, it has been found that dispersive interactions are an essential ingredient so as to attain a satisfactory description of the structure of CA in the solid state.[5,6] Furthermore, calculated energy barriers for direct proton transfer across CA monomers amount to $64-75$ meV per molecular unit,[14,15] yet specific reaction pathways for single and collective proton transfer have not been investigated to date.

Even at the most qualitative level, CA displays a very peculiar phenomenology relative to other organic and inorganic ferroelectric materials such as vinylidene fluoride (VDF) and potassium dihydrogen phosphate (KDP).[10] In the case of VDF, for example, high coercive fields of *ca* 1200 kVcm$^{-1}$ are required given the rather large size of the molecular units associated with permanent electric dipole moments in the lattice. In KDP, ferroelectriciy is believed to arise from collective proton transfer, a phenomenon facilitated by its extended three-dimensional crystal structure.[10] CA constitutes a very different case, as attested by much-lower coercive fields relative to other molecular ferroelectrics (14 kVcm$^{-1}$), as well as by a characteristic (accordion-like) pseudo-layered structure where neither molecular reorientations nor collective proton motions in three dimensions are expected to play a role. In spite of its rather small molecular size, CA also exhibits a surprisingly high spontaneous polarization (∼30 $\mu$C cm$^{-2}$) *increases monotonically* with temperature up to at least 400 K.[1,9] Furthermore, calorimetric studies have not detected any phase transitions from liquid-helium temperatures to the known decomposition temperature of the material around 450 K. Microscopic knowledge of this temperature dependent ferroelectricity is important due to its potential applications as organic pyroelectric material in carbon based electronics.[16] In a previous study,[7] ND and DFT-based molecular dynamics (MD) simulations were used to explore the structure and dynamics of CA as a function of temperature, respectively. From the MD simulations, it was found that medium-range order associated with O-H and O-O correlations is affected by an increase in temperature, although the characteristic long-range layered structure of solid CA remains unaltered. Notwithstanding these initial efforts, a microscopic understanding of the origin and peculiar phenomenology that characterizes the ferroelectric response of solid CA remains elusive.

To fill this gap in our current understanding, in this paper we have used a combination of high-resolution INS and first-principles DFT calculations relying on a phonon picture of the material within the quasiharmonic approximation (QHA). The development of structural instability due to increase in temperature is explored from this phonon pictures. Thermal behaviour of proton motions are investigated using thermodynamic analysis and Debye model on the INS spectra as well as by a detailed exploration of minimum-energy paths associated with both single-particle and collective proton transfer. These results are complemented by calculations of the spontaneous polarisation using the Berry-phase method for comparison with available experimental data. A correlation of thermal-motion induced strain with the spontaneous polarisation is also presented.

## 2 Methodology

Following the work of Braga *et al.*,[17] CA single crystals were obtained from commercially available powders (Sigma Aldrich No. 391700, 98% purity) dissolved in an aqueous solution and kept at all times in an inert helium atmosphere. Successive crystallization runs were carried by slow evaporation over a period of several weeks to obtain well-defined millimeter-sized platelets.

INS spectra as a function of temperature were measured on the IN1-Lagrange neutron spectrometer at the Institut Laue-Langevin (France).[18] To this end, a single crystal of mass 100 mg was ground to a fine powder, and kept in an inert helium atmosphere at all times and away from direct exposure to ambient light so as to prevent unwanted oxidation and decomposition. On IN1-Lagrange, an incident-energy range of 216-3500 $cm^{-1}$ was achieved by means of a doubly focused Cu(220) monochromator reflection, resulting in a relative spectral resolution of $\Delta E/E \sim$ 2-3%, where $E$ denotes energy transfer. In this configuration, the accessible $E$ range was 180-3465 $cm^{-1}$ with a fixed final energy of 36 $cm^{-1}$. INS data were collected in 50 K intervals over the temperature range 5-300 K.

Electronic-structure calculations were performed with the DFT code CASTEP.[19] For all calculations, optimized norm-conserving pseudopotentials[20] generated with the Perdew-Burke-Ernzerhof (PBE)[21] functional within the generalized-gradient approximation (GGA) have been used. Dispersion corrections to the PBE functional (PBE+D) were included following the methodology of Tkatchenko and Scheffler (TS).[22] It has been found that using the functionals for dispersion corrections proposed by Grimme[23] does not change values of calculated phonon frequencies. A plane-wave cutoff of 800 eV and a Brillouin-zone (BZ) sampling of 6x6x3 k-points (18 points when symmetry-reduced) were found to be sufficient to converge energy and atomic forces below 9.6x$10^{-3}$ eV/ion and 1.0x$10^{-3}$ eV/Å, respectively. Self-consistent single-point energy minimizations used a tolerance of 2.5x$10^{-9}$ eV. Geometry optimizations were performed on local coordinates on experimentally obtained unit cell structures with a force tolerance of 1.0x$10^{-3}$eV/Å using the Broyden-Fletcher-Goldfarb-Shanno (BFGS) algorithm.

In the subsequent phonon calculations, normal mode frequencies and eigenvectors of the resulting minimum-energy structures were calculated via diagonalisation of dynamical matrices computed using density-functional perturbation theory (DFPT) and linear-response methods.[24] Using DFPT, phonon dispersion calculations were performed on a total of 8-$q$ points followed by interpolation to obtain a total of 209 $q$-points within the first BZ. Within the QHA approximation, thermal effects on phonon structure were obtained via the use of experimentally determined unit-cell parameters at a given temperature. INS spectra were obtained from calculated eigenvectors and eigenenergies using the newly implemented abINS algorithm in Mantid.[25,26] Calculated INS spectra included fundamentals as well as overtone and combination bands up to fourth order. Mean-square displacements (MSDs) were calculated from the anisotropic displacement parameters (ADPs) obtained from thermodynamic analysis using phonon frequencies and wavevectors as implemented in CASTEP.

In line with a previous study of proton transfer in crystalline squaric acid[27], three functionals (PBE[21], optPBE-vdW[28], and vdW-DF2[29]) were used for nudged-elastic-band (NEB) calculations,[30] for direct comparison of optimized structures against experimental lattice parameters. The best agreement was found via the use of vdW-DF2 and, therefore, this functional was used for minimum-energy-path (MEP) calculations. Unit-cell polarizations were calculated using the Berry-phase method,[31] as recently implemented in CASTEP.

## 3 Results and Discussion

### 3.1 Thermal behaviour of proton motions

Figure 2 shows INS spectra of solid CA over the temperature range $5-300$ K. Qualitatively speaking, the two most prominent peaks located at 850-900 $cm^{-1}$ undergo a relatively mild red-shift with increasing temperature. This effect is accompanied by an overall decrease in spectral intensity across the entire energy-transfer range, although we note that most well-defined features are still noticeable up to room temperature. From these data, we find no evidence for the presence of phase transitions over this temperature range, in agreement with previous ND experiments.[7] On the basis of previous works,[5–7] the strong doublet near 850-900 $cm^{-1}$ is assigned to out-of-plane H-O–H bending motions associated with the two distinct HB protons in crystalline CA. The observed splitting of 64 $cm^{-1}$ at 5 K also tells us that the potential seen by H(T) is sensibly flatter than that seen by H(H) atoms.

Figure 3 reports the evolution of the peak position of these two spectral features as a function of temperature, including a comparison with QHA predictions. The observed decrease in mode frequency is monotonic and, therefore, consistent with the absence of phase transitions over this temperature range. In terms of relative changes, INS mode frequencies decrease in a similar fashion up to 200 K. Above this temperature, the mode associated with H(H) appears to exhibit relatively more decrease than the mode associated with H(T) indicating that the mode corresponds to the terrace type hydrogen bond may be responsible to hold the solid state structure of CA at high temperature.

The calculate change in H-O–H bending frequencies with temperatures shown in Fig. 3 along the experimental results predict the same qualitative trends, although, the calculated relative decrease in mode frequencies is far less pronounced than

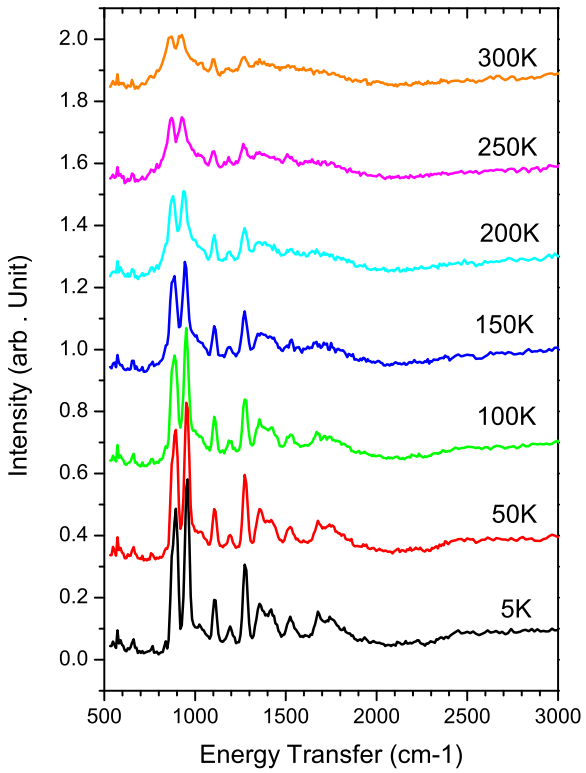


**Fig. 2** INS spectra as a function of sample temperature. For further details, see the text.

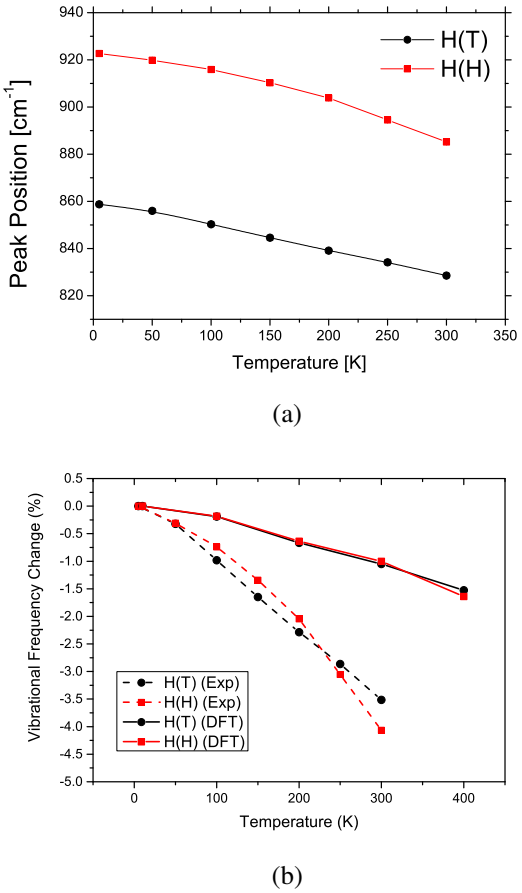


**Fig. 3** Temperature evolution of the mode energies associated with out-of-plane H-O–H bending motions in CA: (a) net change in mode energies obtained from the INS data; (b) percent change relative to the lowest temperature investigated in this work – both INS data and QHA predictions.

observed experimentally and we can trace back these quantitative differences to the prediction of stiffer HBs in the PBE+D calculations, where it has been shown that HB and OH bond lengths are 8% shorter and 3% longer, respectively, than those observed with ND.[7] The thermal expansion co-efficient of CA is $\sim 10^{-5}$/K obtained from ND experiments suggests that anharmonic contributions to vibrations are not negligible. Going beyond the QHA , however, would require recourse to other methodologies like MD, beyond the scope of the present work.

More quantitative estimates associated with the onset of atomic motions with temperature can be obtained from the INS data. To this end, we recall that one of the primary merits of neutron spectroscopy is that the intensity of a particular INS mode is directly related to the dynamic structure factor $S(Q,E)$. For a crystal containing N atoms in the unit cell, the following relation describes the contribution of the single-quantum excitation of normal mode $m$ with energy $E_m$ to the overall $S(Q,E)$ at temperature $T$ [32–34],

$$S_m(Q,E) = \sum_i^N \frac{\hbar^2 |\mathbf{Q}\cdot\mathbf{e}_{i,m}|^2}{2M_i E_m} exp\{-2W_i(Q,T)\}\delta(E-E_m) \quad (1)$$

where, $\mathbf{e}_{i,m}$ is the eigenvector of atom $i$ in mode $m$, $M_i$ is the mass of atom $i$, $\mathbf{Q}$ is the momentum-transfer vector, and $W(Q,T)$ is the Debye-Waller factor at temperature $T$. For an orientationally averaged crystal, the (temperature-dependent) Debye-Waller factor is related to the mean-square displacement (MSD) $u^2$ via the relation $2W = \frac{1}{3}Q^2 < u^2 >$.[35] For an inverted-geometry INS spectrometer like IN1-Lagrange, $Q^2$ and $E$ are proportional to each other. Since $Q$ and $U_m$ are vector quantities, a powder averaging has been applied in this calculation following standard methodology. [32]

Our earlier work has established that the doublet associated with out-of-plane H-O–H bending motions in CA is dominated by proton motions.[6] Taking this information into account, INS intensities for that given normal mode at two different temperatures $T_1$ and $T_2$ obey the following relation,

$$\frac{S_m(T_1)}{S_m(T_2)} = \frac{E_2}{E_1}\frac{e^{-2W(T_1)}}{e^{-2W(T_2)}} \quad (2)$$

where $E_i$ and $S_m(T_i)$ are the energy and INS intensity, respectively, of the normal mode at temperature $T_i$ and the small (%) changes to the second order of the dot product of orientationally averaged momentum transfer $Q$ and eigenvectors associated with mode energy $e_m$ as a function of temperature has been neglected.

Applying the criteria of inverted geometry instrument on Debye-Waller factor, from Eq.2 we get:

$$E_2 < u_2^2 > \; - \; E_1 < u_1^2 > = \frac{3\,\hbar}{2\,m}\, ln\Big[\frac{E_1 S(T_1)}{E_2 S(T_2)}\Big] \quad (3)$$

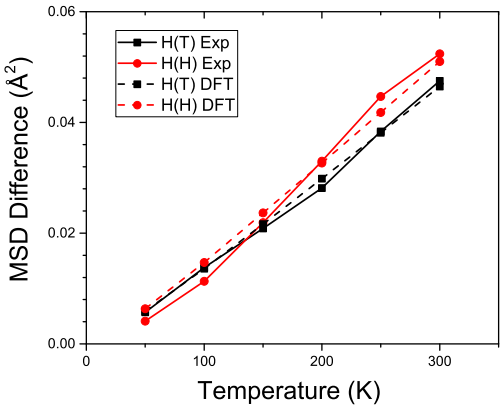


**Fig. 4** Temperature dependence of change in MSDs for H(H) and H(T) ions with respect to at T=5 K. Solid lines with symbols are obtained from INS data and dashed lines from DFT calculations. For further details, see the text.

where $u_i^2$, $E_i$ and $S(T_i)$ are the MSD, energy transfer and INS intensity, respectively, of the mode at temperature $T_i$. If we neglect the temperature dependence of the normal mode energy with respect to its energy value, the Eq. 3 reduces to :

$$< u_2^2 > \; - \; < u_1^2 > = \frac{3\,\hbar}{2\,mE_1}\, ln\Big[\frac{S(T_1)}{S(T_2)}\Big] \quad (4)$$

where $E_1$ is the energy of the normal mode at base temperature.

Figure 4 reports temperature dependent differences in MSDs obtained from the INS data of the doublet and the same for hydrogens from DFPT calculations with respect to those at 5 K. In the latter case, MSDs have been obtained from the diagonal elements of ADP tensors calculated within the QHA. Both datasets agree with each other within 5%, a strong indication that the softening of these two modes is dominated from respective hydrogen motions. Moreover, since difference of MSDs are plotted, the displacements associated with zero point vibrations are eliminated to a certain extent.[36] The calculated MSD using DFPT corresponding to zero-point motion of H(H) and H(T) are $1.648 \times 10^{-2}$ Å and $1.657 \times 10^{-2}$ Å, respectively, suggesting its effect is negligible at room temperature. It is found that MSDs of both H(H) and H(T) increase with temperature in an identical manner, however, characteristic MSDs at room temperature is $\sim 0.05$ $Å^2$, indicating that both types of protons undergo a similar degree of thermal excitations, still well below characteristic jump-distances associated with proton transfer ~1.5 Å between two molecules. These MSDs are consistent with those required for the deformation of the crystal leading to transition from a non-centrosymmetric (ferroelectric) to centrosymmetric (paraelectric) structure,[14] as typically

observed in inorganic ferroelectics such as $BaTiO_3$.[38]

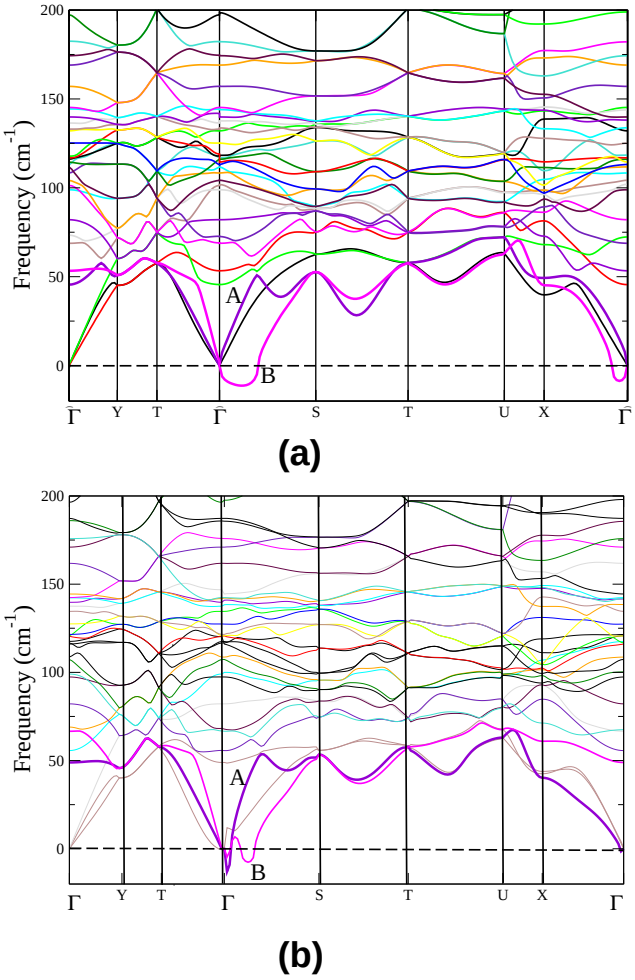


**Fig. 5** QHA phonon dispersion curves across the Brillouin zone for CA at 10 K (a) and 300 K (b). Potential soft modes are labeled as A and B. For further details, see the text.

A more detailed look of calculated MSDs reveals that both H(H) and H(T) show a consistent directionality of displacements at all temperatures. MSDs along the crystallographic *a*-axis are dominant, with values being 2% and 1.5% larger than those along the *c* and *b* directions, respectively. These results evince that in absence of any external field intermolecular proton transfer involving H(H) is less likely because these bonding motifs run preferentially along the *c*-axis and the net polarization per unit cell is preferentially aligned along this direction. Similar considerations apply to HBs associated with H(T), running at *ca* 45 ° relative to both *a* and *b* directions. These results, therefore, strongly suggest that the relation between MSDs and spontaneous ferroelectric response in CA is far from being trivial and does not seem to involve the possibility of proton transfer along HBs without application of any external electric field.

Phonon dispersion often contains important information about inter-atomic forces and effect of motion of atoms on stabilization of lattice structures. We have calculated full phonon dispersion of CA for four different temperatures, 10 K, 100 K, 200 K and 300 K within the QHA. The phonon dispersion in the low vibrational frequency region for structures at 10 K and 300 K are shown in Fig. 5. From Fig. 5 it is found that soft phonon modes exist near the Γ point in the dispersion plot in the $\Gamma - S$ branch. These soft phonons are absent in cell optimised lattice structures. Two modes are identified as responsible for soft modes. These two modes are indicated by **A** and **B** on the Fig. 5. Mode **A** corresponds to the rocking motion of molecular units in sheets, where two adjacent molecular units on the same sheet connected by H(T) rocks in the same direction, but molecular units connected through H(H) rocks in opposite directions forming a sheering motion between sheets. The mode **B** corresponds to rocking motion of all two adjacent molecular units in opposite directions. Instability of the mode **B** in both low (10 K) and high (300 K) temperatures indicates that the experimentally obtained unit cell has structural instability governed by the motion of adjacent molecular units is possible even at low temperatures. This result also predicts that that rocking motions on adjacent sheets may be responsible for the distortion of the lattice structure during transition from paraelectric to ferroelectric phase, change in phase at the high temperature or melting of solid CA.

### 3.2 Proton-transfer pathways

As proton transfer is considered as a mechanism of ferroelectricity in presence of applied field in organic crystals, to understand the mechanisms in the CA crystal the minimum energy paths (MEPs) for proton transfer have been calculated, as shown in Figs. 6-7, using NEB calculations[30]. Fig. 6 shows the MEPs from the three different functionals PBE, optPBE-vdW and vdW-DF2. There is clearly a very large difference between the functionals, with PBE predicting the smallest barrier and shortest reaction coordinate (cumulative displacement of atoms along the MEP), while vdW-DF2 predicts the highest barrier and longest reaction coordinate. This agrees with previous DFT studies of squaric acid[27], where, furthermore, vdW-DF2 was found to agree best with explicitly correlated MP2 and RPA calculations in terms of the barrier height for proton transfer.

The collective proton transfer event shown in Fig. 6, which corresponds to a polarity reversal of the unit cell, is composed of two steps. First, all four H(T)-atoms jump across the H-bond (first barrier for vdW-DF2), followed by all four H(H)-atoms (second barrier for vdW-DF2). However, this is not the only possible mechanism, as shown in Fig. 7. In this figure only

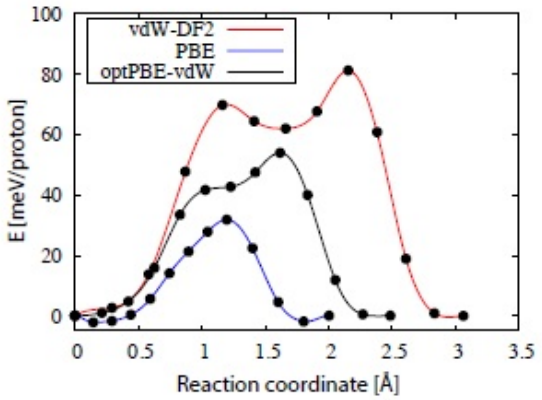


**Fig. 6** Minimum-energy path for complete unit cell proton transfer (polarization reversal) in CA, showing a comparison of PBE, optPBE-vdW and vdW-DF2 functionals, obtained by the nudged elastic band (NEB) method[30]. In this collective proton transfer mechanism, first the 4 H(T)-atoms transfer, followed by the 4 H(H)-atoms.

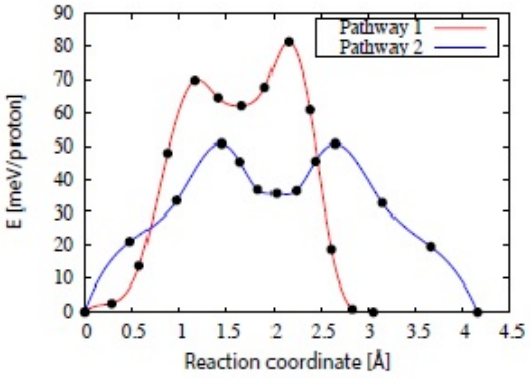


**Fig. 7** Minimum energy path for complete unit cell proton transfer in CA, showing two alternative pathways found by NEB calculations and the vdW-DF2 functional. Pathway 1 is the same as shown in Fig. 6, while Pathway 2 is composed of 4 steps: a) transfer of two H(T)-atoms in neighboring planes; b) somewhat asynchronous transfer of two H(H)-atoms; c) somewhat asynchronous transfer of the remaining two H(H)-atoms; d) transfer of the final two H(T)-atoms.

vdW-DF2 results are shown, both for the two-step mechanism shown in fig. 6 and for a different mechanism which leads to a symmetric double barrier with lower barrier height but longer reaction path than the first mechanism. This second mechanism is composed of four steps. First two H(T)-atoms in neighboring planes jump across the H-bond, then two H(H)-atoms jump (asynchronously, in the upper plane), then the second two hinge H-atoms jump (asynchronously in the lower plane), and finally the final two H(T)-atoms jump. Both mechanisms can be expected to play a role in polarity reversals in croconic acid, which can be realized by applying strong electric fields to the crystal. The barrier heights of all other combinations of pathways are found considerable higher in energies than pathways discussed here. The amount of required displacements for protons to do these collective jumps found in MEP calculations are, however, larger than MSD calculated from INS spectra and from values of ADP as shown in Fig. 4, therefore not possible without an electric field.

### 3.3 Polarization and ferroelectricity

Using our DFT results, we can investigate further the microscopic origin of ferroelectricity in CA. To this end, Fig. 8 shows a comparison between our predictions for the DC-permittivity along the three crystallographic directions and available experimental data as a function of temperature[1]. The agreement between these two datasets is satisfactory in terms of general trends, including an overall insensitivity to temperature. The DC-permittivity along the *c*-axis dominates the response, followed by very similar contributions along the *b* and *a* direc-

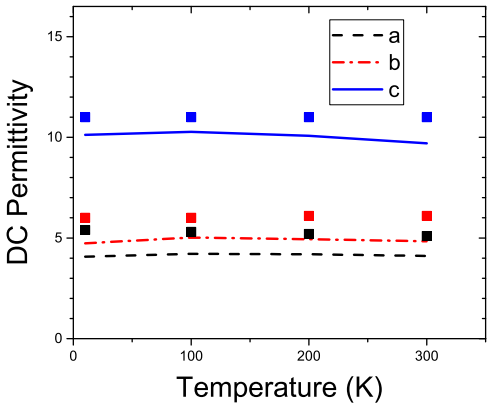


**Fig. 8** Temperature dependence of experimental (symbols) and calculated (lines) dc-permittivities along the three crystallographic directions. Experimental data have been taken from Ref. 1.

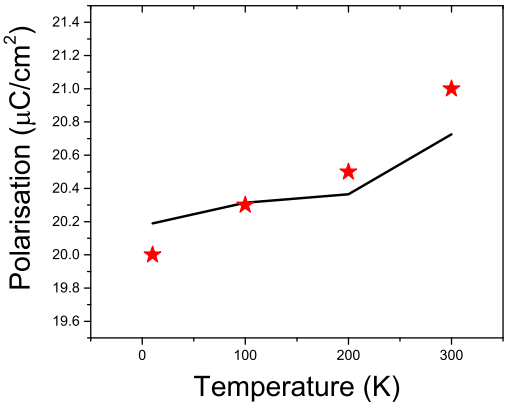


**Fig. 9** Temperature dependence of the spontaneous bulk polarisation along the crystallographic *c*-axis, calculated using the Berry-phase method. Experimental data taken from Ref. 1 are given as scattered symbols. For further details, see the text.

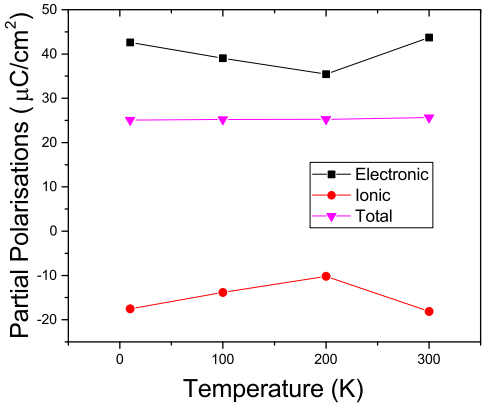


**Fig. 10** Temperature dependence of the partial polarisations along the crystallographic *c*-axis, calculated using the Berry-phase method.

tions. This trend is reproduced by the DFT calculations, including the relative decrease by *ca* a factor of two when considering absolute values along the *c*-axis relative to *a* or *b*. At a more quantitative level, we note that the DFT calculations consistently underestimate the value of these directional permittivities by 10-20 % relative to experiment. This discrepancy may be due the breakdown of the QHA used in calculations.

Very similar trends as a function of temperature are also found for calculated Born effective charges, a quantity that has been correlated to ferroelectric response in CA[5,6] and other materials.[37–41]. These results show that the low frequency phonons, which contribute maximum in the value of Born effective charges, don't change their values with the temperature dependent lattice structures.

Using the Berry-phase method, our DFT calculations can also be used to obtain quantitative predictions of the net spontaneous bulk polarization $P_s$ for comparison with previous studies. Using this formalism, $P_s$ can be decomposed into two separate contributions, that is,

$$P_s = P_{el} + P_{ion} \tag{5}$$

where $P_{el}$ and $P_{ion}$ correspond to electronic and ionic contributions, respectively.[31,38] These data are shown in Fig. 10.

It is found that the calculated value of polarisation for the cell-relaxed ground state structure is 21.75 $\mu C/cm^2$, which is a very good comparison with experimental value 20 $\mu C/cm^2$ [1] and calculated values reported previously at low temperatures.[3] Calculated values on experimental cell structures are, however, 17% higher being consistent with the recently reported experimental and calculated values, c.a. $28-31$ $\mu C/cm^2$, at room temperature.[9] Since there is no temperature dependent data in the recent report, those calculated values are shifted by 4.9 $\mu C/cm^2$ to compare with previously reported temperature dependent experimental values [1] in Fig. 9. In this plot the component of the polarisation tensor along the *c* direction of the crystalline lattice is shown, since all other components are negligibly small. The polarisation of the centrosymmetric phase has come out zero for all temperatures. The values of polarisations obtained experimentally are plotted on the same plot by scattered Astrix. Although calculated temperature dependent polarisations doesn't agree quantatively with experiments, the trend of change in ferroelectricity with temperature, as shown in Fig. 9, is in qualitative agreement with experiments.[1]

The increase in computational polarisation values calculated on experimental lattice parameters may be due to the fact that there is about 3% expansion of the volume of the unit cell with respect to that of experiments during optimisation of cell parameters which reduces total energies by 12.5 meV per formula unit. Further $\sim 8\%$ difference in HB distances in between the local-coordinate optimised structures and in the experimental structures across temperature range 10 K-300 K has been reported previously. [7] These differences in structural parameters may introduce an effective strain which is consistent with the finding (Fig. 5) of soft phonons near $\Gamma$ point suggesting structural instability. This effective strain may also responsible for increase in ferroelectricity,[38] It is also reported that experimental polarisation values are not unique and depend on experimental conditions.[9] More on the relationship between the lattice strain with ferroelectricity is discussed below.

As shown in Fig. 10, the electronic, components of the Berry-phase polarisations are about 4 times higher than that of the ionic components. This indicates the electronic or quantum

mechanical nature of the ferroelectricity. The trend of change of electronic and ionic components of polarisation with temperature is just opposite, therefore, compensating each other's trend to a certain extent. However, the overall trend is dominated by the electronic component. Since the values of electronic and ionic components are results of short range and long range interactions, respectively, the temperature dependent polarisation is a fine balance between these two. The indeterminacy component, i.e., the polarisation-quantum, is almost double of that of the electronic component, however, that term doesn't play any role in the value of polarization in this case.

The spontaneous polarization, $P_s$, is related with the Born effective charge by,

$$P_s = \frac{|e|}{V}\sum_{i=1}^{N} Z_i^* \cdot d_i \tag{6}$$

where, $Z_i^*$ and $d_i$, are the Born effective charge and the displacement of $i$th atom, respectively; $N$ is the number of atom per unit cell and $V$ is the volume of the unit cell. [39] As mentioned above, since Born effective charge on H(H), the atom responsible for ferroelectricity, [6] is independent of temperature, the increase in ferroelectricity with temperature suggests the increase in displacements of that H(H) along the polarisation axis, c. As the volume of the unit-cell is inversely correlated with polarisation, a significant increase in displacement of H(H) is required to compensate the increase in volume due to thermal expansion.

The correlation of polarisations with structural parameters, such as displacement of proton, via change in O-H bond lengths, becomes inconclusive, because although polarisation is increasing with temperatures, O-H bond lengths decrease with increasing temperatures. [7] On the other hand HB lengths and lattice parameters increases with temperature.

Since position vectors are time averaged parameters, we correlate polarisations with c-axis lattice vector in the analysis. In Fig 11 experimental polarisations obtained from Ref. 1 and Berry-phase calculated polarisations with a shift of 4.9 $\mu C/cm^2$ are plotted against the experimentally obtained temperature dependent lattice parameter c and in-plane strain. The in-plane strain , $\varepsilon$ has been calculated as $(d_{||} - d_0)/d_0$ , where $d_{||} = \sqrt{a^2+b^2+c^2}$ and $a$, $b$ and $c$ are temperature dependent crystallographic lattice parameters reported previously [7]; and $d_0$ is the the value of $d_{||}$ at base temperature. A significant qualitative agreement have been found among these plots. Further to the increase in polarisation with increasing in-plane strain, a clear almost-linear relationship with these parameters are there. The temperature dependent spontaneous polarisation, $P_s(T)$ , is modeled with strain as $P_s(T) = P_0(1+\lambda\varepsilon(T))$, where $P_0$, $\varepsilon(T)$, and $\lambda$ are the polarisation at base temperature, in-plane strain at temperature T, and a parameter, respectively. As shown in Fig. 11 it is found that experimentally obtained polarisation

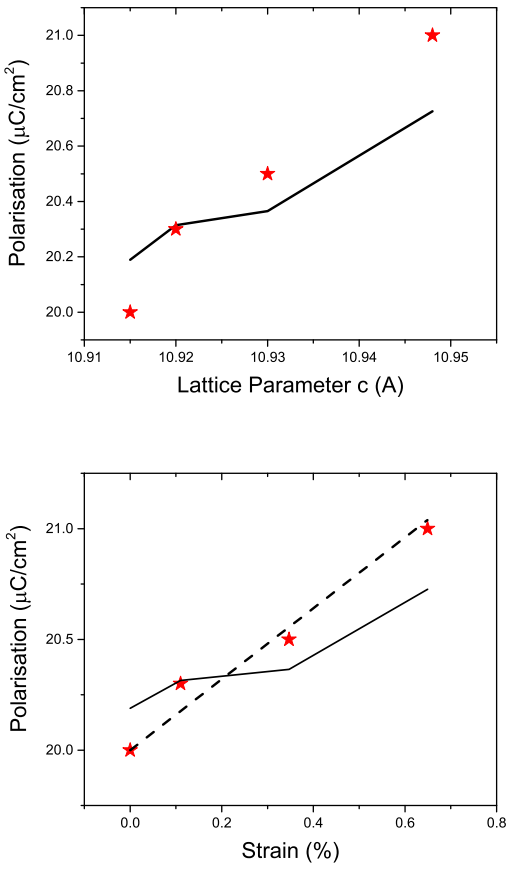


**Fig. 11** The temperature dependent polarisations with (upper plot) lattice parameter c and (lower plot) in-plane strain are correlated. Calculated polarisations (solid line) shifted by 4.9 $\mu C/cm^2$ are plotted with experimental polarisations (symbols) and linear model (dashed line). Experimental data have been taken from Ref. 1. For further details, see the text.

is almost linear with strain, when λ is 8.0. For the polarisation calculated by Berry phase method λ is 4.0. This almost-linear correlation is significant and consistent to other findings in solid-state ferroelectricity in perovskites, because a perfectly linear correlation of ferroelectricity with strain is rare [38].

In a phenomenological dipole model, since the ferroelectricity is found only along crystallographic c-axis, the increase in HB length due to thermal expansion of lattice increases effective dipole moment between the H(H) and the respective oxygen across the strong HB bond along that axis. MSD displacements due to thermal fluctuations, on the other hand, is found only perpendicular to the c-axis. The latter displacements apply additional component of strain on H(H) leading to increase in polarisations further. The dissimilar expansion of a, b and c lattice parameters, as reported earlier [7], causes structural distortions and is the origin of in-plane strain. The signature of this distortion and subsequent strain is also predicted through the plot of phonon dispersion in Fig. 5. The constrained motion of proton along the polarisation axis is significant, because this helps to retain the strong HBs motif even at high temperature. This constrained dynamics of protons along with the lattice distortion due to dissimilar thermal expansion of the lattice is predicted as the microscopic origin of increase in ferroelectricity of CA with temperature. This knowledge may help in designing room temperature ferroelectrics from organic layered materials by applying suitable strain internally or externally.

## 4 Conclusions

Temperature dependent vibrational properties of solid CA have been investigated to understand the influence of temperature on structure and dynamics of hydrogen bonds and the ferroelectricity of CA. Temperature dependent INS experiments along with First principles lattice dynamics calculations within the framework of DFT were presented to understand the structure-dynamics-ferroelctricity correlations. Three important conclusions are drawn from this investigations:

- INS experiments show that the frequencies and intensities of high-intensity INS doublet observed at an energy transfer of ca. 900 $cm^{-1}$ decreases with increase in temperature. The decrease in frequencies of these two modes, corresponding to the out of plane motion of two different types of hydrogen bonds located at the hinge and the terrace positions of the pleated structure are reproduced qualitatively through DFT simulations within QHA. Temperature dependent shift in frequencies predicts the weakening of both HBs. The hinge type HBs soften relatively faster above 200 K indicating that the mode corresponding to the terrace type hydrogen bond may be responsible to hold the solid state structure of CA at high temperature. The calculations within QHA, however, underestimated this shift due to overestimation of HB strength and the break down of QHA at high temperature. From the calculations of phonon dispersion at 300 K, softening of the two modes corresponding to shear motion of two sheets against each other and to the rocking motion of molecular units in sheets, are obtained. Softness of these two modes indicates that long range shear or rocking motions of molecular units may be responsible for temperature dependent properties of CA .

- The temperature dependent MSDs of both hydrogens, calculated from intensities of temperature dependent INS spectrum, are compared within 5% of the calculated values from ADP tensors using DFT. These displacements are, however, far too low from what is required to transfer a proton to the neighbouring molecular unit in absence of any electric field. From these values and directionality of displacive motion of hydrogen atoms obtained from calculated ADP, it is predicted that in absence of any external field, proton transfer along polarisation axis, c, is unlikely. The constrain motion along *c*-axis, however, helps to retain strong HB motif of CA structures at high temperatures. Possible pathways of the proton transfer between molecular units of CA, which may occur due to application of an external electric field, have also been explored to find out the shortest pathways for proton transfer.

- The values of temperature dependent net spontaneous polarisation, calculated using Berry-phase approximation, qualitatively agree with experiments. It is found that the ferroelectricity is quantum mechanical in nature with 20% contributions from long range ionic structures. The microscopic analysis of the polarisation reveals that the inhomogeneous thermal expansion of lattice introduce extra strain on the hydrogen bond structure of CA leading to high ferroelectricity above room temperature. An almost-linear relationship between in-plane strain and ferroelectricity has been found.

It is predicted that these microscopic knowledge may help in designing room temperature ferroelectrics from organic layered materials.

## Acknowledgments

We thank Dr. J. Tomkinson for many useful and enjoyable discussions. The Institut Laue-Langevin is acknowledged for the provision of beam time, and the UK Science and Technology Facilities Council e-Science Department for continued access to the SCARF cluster at the Rutherford Appleton Laboratory. Some of the computations have been performed on the UK National Supercomputing Facility HECToR, and ARCHER (http://www.archer.ac.uk) via our membership of the

UK HEC Materials Chemistry Consortium funded by EPSRC grants EP/D504872 and EP/L000202.

## References


1 S. Horiuchi, Y. Tokunaga, G. Giovannetti, S. Picozzi, H. Itoh, R. Shimano, R. Kumai, and Y. Tokura: Nature **463** 789 (2010).

2 D. A. Kunkel, J. Hooper, B. Bradley, L. Schlueter, T. Rasmussen, P. Costa, S. Beniwal, S. Ducharme, E. Zurek, and A. Enders, J. Phys. Chem. Lett., **7**, 435 (2016).

3 Y. Cai1, S. Luo, Z. Zhu and H. Gu, J. Chem. Phys., *139*, 044702 (2013).

4 A. Stroppa, D. D. Sante, S. Horiuchi, Y. Tokura, D. Vanderbilt, and S. Picozzi: Phys. Rev. B **84** 014101 (2011).

5 F. Fernandez-Alonso, M. J. Gutmann, S. Mukhopadhyay, D. B. Jochym, K. Refson, M. Jura, M. Krzystyniak, M. Jimenez-Ruiz, and A. Wagner: J. Phys. Soc. Japan, **82**, SA001 (2013).

6 S. Mukhopadhyay, M. J. Gutmann, M. Jura, D. B. Jochym, M. Jimenez-Ruiz, S. Sturniolo, K. Refson, and F. Fernandez-Alonso, Chem Phys, **427**, 95 (2013).

7 S. Mukhopadhyay, M. J. Gutmann, and F. Fernandez-Alonso, Phys Chem Chem Phys, **16**, 26234 (2014).

8 K. Iwano, Y. Shimoi, T. Miyamoto, D. Hata, M. Sotome, N. Kida, S. Horiuchi, and H. Okamoto, Phys. Rev. Lett., **118**, 107404 (2017).

9 S. Horiuchi, K. Kobayashi, R. Kumai, and S. Ishibashi, Nat. Comm. **8**, 14426 (2017).

10 S. Horiuchi and Y. Tokura Nat. Mat. **7** 357 (2008).

11 J. Seliger, J. Plavec, P. Sket, V. Zagar, and R. Blinc: Phys. Status Solidi B **248** 2091 (2011).

12 V. V. Zhurov and A. A. Pinkerton, Z. Anorg. Allg. Chem., **639**, 1969 (2013).

13 F. Bisti, A. Stroppa, S. Picozzi, and L. Ottaviano: J. Chem. Phys. **134** 174505 (2011).

14 D. Di Sante, A. Stroppa and S. Picozzi : Phys. Chem. Chem. Phys:. **14** 14673 (2012).

15 D. A. Kunkel, J. Hooper, S. Simpson, G. A. Rojas, S. Ducharme, T. Usher, E. Zurek, and A. Enders, Phys. Rev. B, **87**, 041402(R) (2013).

16 N. T. Tien, Y. G. Seol, L. H. A. Dao, H. Y. Noh, and N. Lee, Adv. Mat. **21** 910 (2009).

17 D. Braga, L. Maini, and F. Grepioni: Cryst. Eng. Comm. **6** 1 (2001).

18 A. Ivanov, M. Jiménez-Ruiz and J. Kulda, J Phys. Conf. Series, **554**, 012001 (2014).

19 S.J. Clark,M.D. Segall, C. J. Pickard, P. J.Hasnip,M. J. Probert, K.Refson, and M.C. Payne: Z Kristallogr **220** 567 (2005).

20 A. M. Rappe, K. M. Rabe, E. Kaxiras, and J. D. Joannopoulos: Phys. Rev. B **41** 1227 (1990).

21 J. P. Perdew, K. Burke, and M. Ernzerhof: Phys. Rev. Lett. **77** 3865 (1996).

22 A. Tkatchenko and M. Scheffler: Phys. Rev. Lett. **102** 073005 (2009).

23 S. Grimme, J. Antony, S. Ehrlich and H. Krieg, J. Chem. Phys., **132**, 154104 (2010).

24 K. Refson, S. J. Clark, and P. R. Tulip: Phys. Rev. B **73** 155114 (2006).

25 D. Champion, J. Tomkinson, and G. Kearley: Appl. Phys. A. - Mater. **74** S1302 (2002).

26 K. Dymkowski, S. Parker, F. Fernandez-Alonso, and S. Mukhopadhyay: Physica B (submitted); http://docs.mantidproject.org/nightly/algorithms/Abins-v1.html

27 K. T. Wikfeldt and A Michaelides. J. Chem Phys, **140** 041103 (2014).

28 J. Klimes, D. R. Bowler, and A. Michaelides, J. Phys.: Cond. Matter, **22** 022201 (2010).

29 K. Lee, E D. Murray, L. Kong, B. I. Lundqvist, and D. C. Langreth, Phys. Rev. B, **82** 081101 (2010).

30 G. Henkelman, B. P. Uberuaga, and H. Jonsson. J. Chem. Phys., **113** 9901 (2000).

31 N. A. Spaldin, J. Solid State. Chem. **195**, 2 (2012).

32 P. C. H. Mitchell, S. F. Parker, A. J. Ramirez-Cuesta and J. Tomkinson, *Vibrational Spectroscopy with Neutrons*, World Scientific Pub. London, (2005).

33 F. Fernandez-Alonso and D.L. Price eds, *Neutron ScatteringFundamentals* ,Academic Press, New York (2013).

34 G. J. Kearley, Nuclear. Inst. Method. in Phys. Res. A, **354**, 53 (1995).

35 G. L. Squires, "Introduction to the Theory of Thermal Neutron Scattering", Cambridge University Press (2012).

36 Y. Yang and Y. Kawazoe, Eu. Phys. Lett. **98**, 66007 (2012).

37 N. Dalal, A. Klymchyov and A. Bussmann-Holder, Phys. Rev. Lett, **81** 5924 (1998).

38 K. Rebe, Ch. H. Ahn and J. M. Triscone (Eds. ), *Physics of Ferroelectrics: A Modern Perspective*, Springer-Verlag Berlin Heidelberg (2007).

39 W. Zhong, R.D. King-Smith, and David Vanderbilt: Phys. Rev. Lett., **72** 3618 (1994).

40 H. Sakai,1, J. Fujioka,T. Fukuda, M. S. Bahramy, D. Okuyama, R. Arita, T. Arima,5 A. Q. R. Baron, Y. Taguchi, and Y. Tokura : Phys. Rev. B, **86** 104407 (2012).

41 Ph. Ghosez, J.-P. Michenaud, and X. Gonze Phys. Rev. B, **58** 6225 (1998).